JACS
JOURNAL OF THE AMERICAN CHEMICAL SOCIETY

Communication

pubs.acs.org/JACS

Spatial and Temporal Control of the Diazonium Modification of sp^2 Carbon Surfaces

Paul M. Kirkman, Aleix G. Güell,* Anatolii S. Cuharuc, and Patrick R. Unwin*

Department of Chemistry, University of Warwick, Gibbet Hill Road, Coventry, CV4 7AL, U.K.

Supporting Information

ABSTRACT: Interest in the controlled chemical functionalization of sp^2 carbon materials using diazonium compounds has been recently reignited, particularly as a means to generate a band gap in graphene. We demonstrate local diazonium modification of pristine sp^2 carbon surfaces, with high control, at the micrometer scale through the use of scanning electrochemical cell microscopy (SECCM). Electrochemically driven diazonium patterning is investigated at a range of driving forces, coupled with surface analysis using atomic force microscopy (AFM) and Raman spectroscopy. We highlight how the film density, level of sp^2/sp^3 rehybridization and the extent of multilayer formation can be controlled, paving the way for the use of localized electrochemistry as a route to controlled diazonium modification.

Diazonium modification is recognized as a powerful approach for tailoring the chemical functionality of surfaces.[1] Both metallic[2] and carbon-based substrates (e.g., glassy carbon,[3] highly oriented pyrolytic graphite (HOPG),[4] carbon nanotubes[5]) have been successfully grafted using diazonium salts, and this methodology has recently been extended to graphene.[6] In fact, the use of diazonium chemistry to introduce sp^3 defects into the graphene sp^2 carbon lattice is currently attracting considerable attention[7,8] because such rehybridized defects generate an electronic band gap in graphene,[9] opening up the prospect of graphene-based electronic devices. In principle, one could tune the generated band gap from metallic to semiconducting by controlling the extent and the location of this modification.[10] Thus, spatial and temporal control of the extent of diazonium patterning could provide a means to a full device on a single graphene sheet.[11]

Herein, we demonstrate the localized diazonium modification of sp^2 carbon surfaces, under electrochemical (EC) control, coupled with surface analysis to elucidate the nature and extent of the grafting process. Electrochemically controlled diazonium modification[3,12−14] has advantages over other modification methods[6] in both the level of control that can be achieved, and the shorter time scales required for modification. The focus here is on freshly cleaved HOPG, which has previously served as a model for graphene in diazonium modification[15] and for graphene electrochemistry generally.[16] By confining the modification reaction to the micrometer scale, we are able to controllably pattern the HOPG surface with high spatial precision, an important aspect for the technological development of diazonium functionalization, while also allowing us to identify any influence of surface features (e.g., step edges) on the grafting process.[17] While diazonium patterning is addressed in the literature, via both EC[18,19] and non-EC means,[15,20] methods used hitherto tend to lack the grafting control that we demonstrate herein and may suffer from issues of contamination.[20]

The diazonium grafting process proceeds via the EC reduction of an aryl diazonium cation, producing an aryl radical following the release of N_2. The highly reactive radical can react with the sp^2 carbon surface to form a covalent bond, resulting in rehybridization of the surface atom to sp^3 (summarized in Figure 1a). In this study, the modification reaction is confined to the micrometer scale using scanning electrochemical cell microscopy (SECCM);[21] see Supporting Information (SI) section S1 for details. Briefly, SECCM employs a dual-channel borosilicate glass pipet, pulled to a sharp taper, with the solution of interest (vide infra) and a quasi-reference counter electrode (QRCE) inserted in each channel; these were Pd−H_2 electrodes for this study.[22] By mounting the pipet and sample on *xyz* piezoelectric positioners, a movable, confined-meniscus EC cell is created

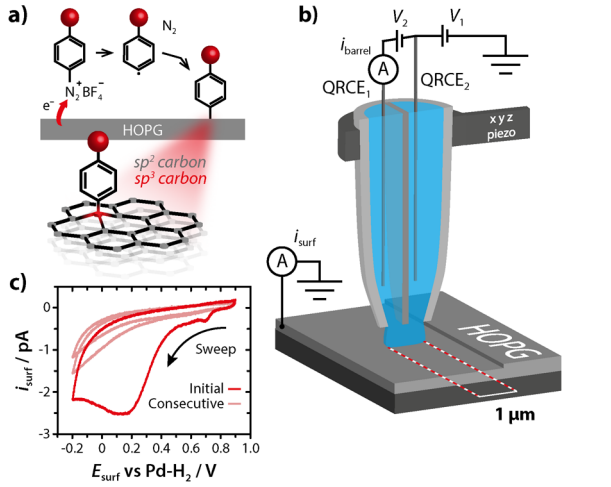

Figure 1. (a) Schematic of the diazonium modification reaction at an HOPG electrode surface, resulting in the production of an sp^3 carbon center in the HOPG surface layer. (b) Schematic representation of the SECCM setup for the localized diazonium modification of HOPG. (c) CV (100 mV s^{-1}) using the SECCM setup on HOPG with 100 μM 4-carboxybenzenediazonium tetrafluoroborate in 25 mM H_2SO_4.

Received: October 11, 2013
Published: December 10, 2013

   dx.doi.org/10.1021/ja410467e | *J. Am. Chem. Soc.* 2014, 136, 36−39

(Figure 1b) that can be accurately positioned on the substrate of interest for an electromodification measurement, before being withdrawn and moved to another location for further measurements. Application of a potential bias (typically 200 mV) between the two QRCEs (V_2 in Figure 1b) induces an ion conductance current across the meniscus (i_{barrel}). By modulating the pipet position normal to the surface, an alternating component of the conductance current develops upon meniscus contact with the surface, enabling precise positioning without the pipet itself touching the surface.[23,24] This pipet-based approach also prevents sample contamination, often introduced through patterning methods requiring more extensive physical contact with the sample (e.g., microcontact printing[20] and lithography[15]) or long periods of sample immersion in solution.[18] Indeed, since spontaneous diazonium reduction/modification can occur at surfaces,[6] there is a need to prevent solution exposure to areas where modification is unwanted, a feature delivered by our approach. During modification measurements, the potential of the surface (E_{surf}) was varied by the adjustment of V_1 (Figure 1b), so that $E_{surf} = -(V_1 + V_2/2)$ vs Pd−H_2,[22] with the resulting EC current measured as i_{surf}.

Figure 1c shows a typical cyclic voltammogram (CV) recorded on HOPG using the SECCM setup, with the aqueous solution in the pipet channels comprising 4-carboxybenzenediazonium tetrafluoroborate (4-CBD) (synthesized in-house, as reported previously[25]), and supporting electrolyte (25 mM aqueous H_2SO_4). A broad irreversible reduction wave is observed on the initial potential sweep (peak potential, E_p = 0.15 V vs Pd−H_2) assigned to the EC reduction of the diazonium molecule. Consecutive scans display a diminished current magnitude since the aryl radicals produced covalently attach to the surface, partly blocking it, and inhibiting further electron transfer (ET). This voltammetric behavior is similar to that obtained for the macroscale EC modification of carbon surfaces using diazonium chemistry,[26] giving confidence that the microscale SECCM measurements mimic the macroscale process.

To demonstrate the localized modification possible using SECCM, and to investigate the effects of substrate grafting potential and modification time on the resulting diazonium film structure, an array of diazonium-modified spots was created on the HOPG surface. For each individual modification, the potential V_1 was set to achieve a desired value of E_{surf} and the pipet approached to the surface (at a rate of 0.05 μm s^{-1}) until meniscus contact, at which point movement stopped automatically and the pipet was held in place for a defined hold time. The pipet was then withdrawn, breaking the EC circuit (meniscus contact) and immediately halting the modification reaction. This process was repeated at fresh areas of the HOPG surface for a range of hold times, typically between 0.5 and 8.5 s, with a 0.5 s increment time, creating an array of 17 diazonium-patterned spots. Such arrays were created at three different E_{surf} values, denoted E_{max}, E_{mid}, and E_{min}, where $E_{max} = E_p$, $E_{mid} = E_p + 150$ mV, and $E_{min} = E_p + 250$ mV, a sequence corresponding to less driving potentials, thereby providing lower rates of aryl radical production.

Figure 2a shows an atomic force microscopy (AFM) image of an array produced at the most driving potential, E_{max}. Clearly visible are 17 well-defined discrete spots, each corresponding to a different hold time of the meniscus at the surface. The reproducible shape and dimensions of the diazonium pattern are determined purely by the pipet opening, ~1 μm in this case (SI, Figure S1), a parameter that can easily be varied from hundreds of nanometers to tens of micrometers,[24] depending on

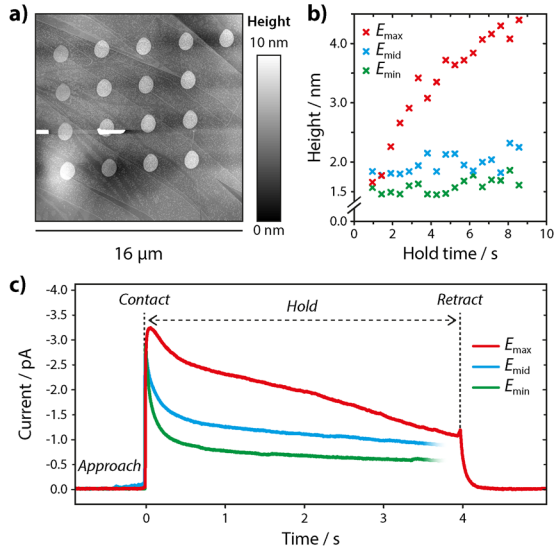

Figure 2. (a) AFM topography image of a typical deposition array created at potential E_{max} using various deposition times. (b) Heights of each deposit (as determined with AFM) as a function of hold time, for the different potentials employed. (c) Three typical current−time transients obtained during the spot deposition, one for each deposition potential.

the spatial resolution desired. AFM images of the arrays obtained at the less driving potentials (E_{mid} and E_{min}), together with an image of pristine HOPG, are presented in SI (Figure S2) and show the same high level of defined modification. Just as noticeable throughout all three arrays is the homogeneity of the deposition within each spot, showing a consistent level of grafting within the modified area.

The use of such a small EC cell, and high-quality HOPG (referred to herein as AM grade, see SI for details), which has a very low step density,[27] means that the HOPG basal surface was primarily targeted during deposition. Very similar modification spots can be seen on both the basal surface (without steps) and the basal surface with intersecting edge plane areas, with no obvious material buildup around step edges. This indicates clearly that the basal surface can easily support the electrogeneration of the radical. It is also unlikely that this basal plane activity (electrochemistry) originates only at basal plane point defects. The average density of such defect sites on HOPG is reported to be between 10^6 and 10^{10} cm^{-2},[28,29] suggesting a maximum of ~100 point defects within each deposition area. Additional macroscale modification measurements were performed on this high-quality HOPG, as well as SPI-3 HOPG, where the step edge density is orders of magnitude higher.[27] Despite these large differences in sample quality, the resulting voltammograms and rate of blocking revealed by repetitive voltammetric cycles appear nearly identical (SI, Figure S3). These findings agree with other recent studies that the HOPG basal surface can easily support a wide range of EC processes.[30,31]

AFM analysis also provides insight on the kinetics of film growth. First, focusing on the array created at the most driving potential, E_{max}, it is evident that multilayer growth is dominant under these conditions, as shown in Figure 2b. The film thickness increases with time (~4 nm after 8.5 s), attributed to electrogenerated aryl radicals reacting with diazonium moieties already attached to the surface.[13,14,32] In contrast, AFM analysis for the two lower modification potentials shows that the spot height within each array remains more or less constant (~2 nm

dx.doi.org/10.1021/ja410467e | J. Am. Chem. Soc. 2014, 136, 36−39

for E_{mid} and 1.5 nm for E_{min}) over the range of time scales investigated (Figure 2b). Note that at all potentials and times examined, the film thickness was more than expected for a monolayer (0.68 nm).[33] Importantly, the pipet used in SECCM provides high intrinsic diffusion rates to the surface,[23] owing to nonlinear diffusion from the tapered pipet design, and this rate is enhanced further via the applied potential between the two QRCEs, leading to migration of the charged diazonium molecule to the surface.[23] Thus, compared to conventional macroscale measurements, film growth rates may be enhanced, an effect also seen in recent diazonium modification experiments on gold ultramicroelectrodes.[2]

To gain further insight on the potential-dependence of the film growth process, current−time transients for each of the spot depositions at the three potentials were examined; typical transients are shown in Figure 2c. Each shows zero current during the *approach* of the meniscus to the surface, an immediate current jump upon meniscus *contact* (owing to diazonium reduction), followed by a current decay during the *hold* step, and a final jump back to zero upon *retraction* of the pipet. Considering first the transient at E_{max}, the initial current decay (<2 s), much longer than the characteristic diffusion time constant of SECCM (~5 ms),[23] is due mainly to transient radical generation, starting at the bare/unreacted sp^2 carbon on the HOPG surface, coupled with some effective blocking of the HOPG surface by electrogenerated radicals. There is a superimposed longer duration decay resulting from the increasingly thick, insulating diazonium layer that is formed, reducing the reactant flux to the electrode surface and hindering electron transfer (ET).

At potentials E_{mid} and E_{min}, the current decay occurs on a longer time scale and is due to a film growth regime where the film density (concentration of molecules in the film) increases with time, rather than the growth of multilayer structures as highlighted by the AFM analysis (Figure 2b). This is corroborated with the electrochemical charge associated with each of the deposition spots, where for E_{mid} and E_{min} the charge increases monotonically with time, but the microspot height remains relatively constant (SI, Figure S4).

We used Raman spectroscopy to further examine the level of diazonium modification of the HOPG surface.[17] The Raman spectrum of bare HOPG (SI, Figure S5) shows a distinct peak at ~1580 cm^{-1}, due to the vibrational mode (G-band) of the sp^2-bonded network. After diazonium modification, a second peak (D-band) develops at ~1350 cm^{-1}, diagnostic of the local sp^3 carbon content of the HOPG surface,[17] and hence the level of diazonium modification. Raman mapping of the diazonium arrays produced at potentials E_{max} and E_{mid}, as representative of the two film growth regimes on the time scale of interest, was performed and plotted as D-band intensity (a and b of Figure 3, respectively). Each map shows distinct features, in positions that correlate with the spots seen by AFM imaging, confirming the covalent attachment of aryl groups at both basal plane, and step edge sites. Corresponding D/G ratio Raman maps showing the same trend are presented in SI (Figure S6). Figure 3c plots normalized D-band intensity for each deposition spot, providing information on the level of sp^3 carbon over the range of hold times investigated. The two different growth regimes at E_{max} and E_{mid} are manifested as different trends in intensity vs time. The D-band intensity at E_{max} shows a short, sharp increase over the first 2 s, attributed to increasing coverage of the HOPG surface, up to a maximum value, beyond which no major change in the Raman signal is seen. Coupled with the AFM data (Figure 2b), this points to a polyaryl multilayer growth process[34] in which the film

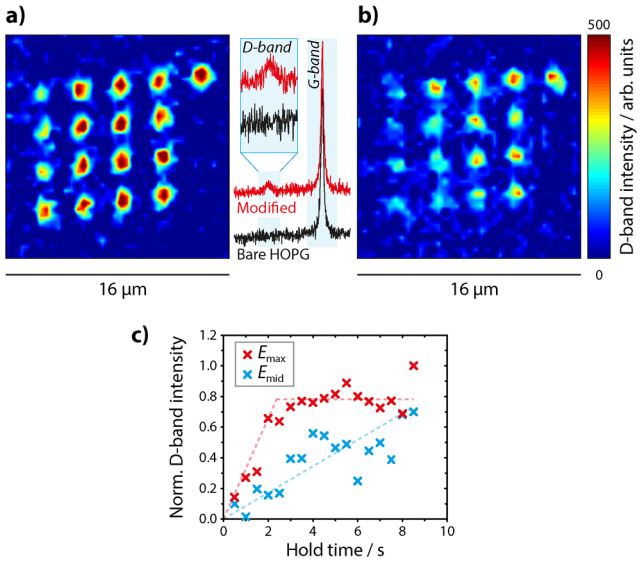

Figure 3. Typical Raman maps plotted as D-band intensity over the surface of the arrays created at potentials E_{max} (a) and E_{mid} (b) along with representative spectra for modified and unmodified areas. (c) Normalized D-band intensity (with respect to maximum D-band intensity measured), plotted for each of the spots as a function of deposition hold time, for the aforementioned maps at both E_{max} and E_{mid}.

thickness increases with time, but the maximum surface coverage is obtained within a short (~2 s) period. In contrast, although the Raman data at E_{mid} shows some scatter (as a result of the laser Raman spot and microdeposit being of similar size), an overall trend of increasing D-band intensity with time is evident, consistent with the interpretation of the AFM and current−time data that the major process at low driving force is simply the increase in concentration of a film of more or less constant thickness. It should be noted, however, that analysis of the Raman data provides only a relative description of the level of sp^3 carbon introduced, because the G-band signal arises from the surface and bulk graphite.

The EC charge associated with the grafting process provides a guide as to the level of surface coverage (Γ) achieved and can be used to give further insight on film density, provided that the grafting efficiency is known. This can be estimated by careful analysis of the CV response during diazonium modification.[12] Using this approach and macroscopic voltammetry we determined an efficiency of s = 92% for the system investigated here (full details given in SI, section S4).

Figure 4a shows Γ (determined from charge) against hold time for all deposition experiments, considering an 8% loss of generated radicals to solution. Additional information can be extracted from these Γ values by also taking into account spot deposition heights, as plotted in Figure 4b. This plot informs on changes in film density with hold time, yielding film density values, and hence provides details on the relative number of sp^3 carbon centers introduced at the sp^2 surface. Depositions performed at E_{max} show a distinct linear trend, suggesting film growth at a more or less constant density, with an estimate of the average film density of 1.7×10^{-9} mol cm^{-2} monolayer^{-1}, a reasonable match with the range expected if all layers were densely packed ($1.2-1.35 \times 10^{-9}$ mol cm^{-2} monolayer^{-1})[4,35] and in very good agreement with previous literature.[6,12] Thus, films produced at such driving potentials mainly appear densely packed, with hold time controlling only the degree of multilayer

dx.doi.org/10.1021/ja410467e | J. Am. Chem. Soc. 2014, 136, 36−39

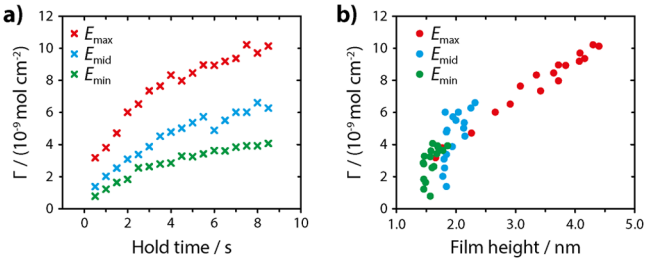

Figure 4. (a) Plots of surface coverage (determined from EC charge with s = 0.92) against hold time for each of the three deposition potentials investigated. (b) Plots of surface coverage deposition height for each of the three deposition potentials.

extension. Only the density values for depositions <2 s deviate below this average value, indicating the film has a lower density at these very short timescales.

In contrast, the densities produced at E_{mid} and E_{min} appear to increase with longer deposition times, as depicted by increasing surface coverage values, despite relatively constant deposition heights (Figure 4b), before beginning to plateau at densities of 1.8×10^{-9} mol cm^{-2} monolayer^{-1} and 1.7×10^{-9} mol cm^{-2} monolayer^{-1} respectively, at the longest hold time investigated. This analysis corroborates conclusions drawn from the AFM and Raman data, which suggested that small driving potentials accessed an initial film-filling regime. This highlights the wide range of film densities, and hence levels of sp^3 carbon, obtainable in the final film through the use of lower modification potentials, and suitable modification times.

To conclude, we have demonstrated the modification of pristine sp^2 basal plane graphite with diazonium compounds, using SECCM to achieve a high-degree of spatial control, with the properties of the resulting modification tuned via the applied potential and meniscus contact time. This approach allows the dominant growth regime to be tuned, and provides access to a range of film densities, with the degree of multilayer formation also controlled.

■ ASSOCIATED CONTENT

Supporting Information

Full experimental details. This material is available free of charge via the Internet at http://pubs.acs.org.

■ AUTHOR INFORMATION

Corresponding Authors

a.g.guell@warwick.ac.uk
p.r.unwin@warwick.ac.uk

Notes

The authors declare no competing financial interest.

■ ACKNOWLEDGMENTS

This work was supported by the European Research Council (No. ERC-2009-AdG 247143-QUANTIF). We thank Dr. Alex Colburn and Kim McKelvey for instrumentation design and development, Prof. R.L. McCreery for providing high-quality HOPG and Guohui Zhang for AFM assistance. We acknowledge financial support from Lubrizol to P.M.K. and the EPSRC (EP/H023909/1) for funding A.G.G. A Chancellor's International Scholarship from the University of Warwick was awarded to A.S.C.

■ REFERENCES

(1) Bahr, J. L.; Yang, J. P.; Kosynkin, D. V.; Bronikowski, M. J.; Smalley, R. E.; Tour, J. M. *J. Am. Chem. Soc.* **2001**, *123*, 6536.
(2) Munteanu, S.; Roger, J. P.; Fedala, Y.; Amiot, F.; Combellas, C.; Tessier, G.; Kanoufi, F. *Faraday Discuss.* **2013**, *164*, 241.
(3) Delamar, M.; Hitmi, R.; Pinson, J.; Savéant, J. M. *J. Am. Chem. Soc.* **1992**, *114*, 5883.
(4) Liu, Y. C.; McCreery, R. L. *J. Am. Chem. Soc.* **1995**, *117*, 11254.
(5) Strano, M. S.; Dyke, C. A.; Usrey, M. L.; Barone, P. W.; Allen, M. J.; Shan, H. W.; Kittrell, C.; Hauge, R. H.; Tour, J. M.; Smalley, R. E. *Science* **2003**, *301*, 1519.
(6) Bekyarova, E.; Itkis, M. E.; Ramesh, P.; Berger, C.; Sprinkle, M.; de Heer, W. A.; Haddon, R. C. *J. Am. Chem. Soc.* **2009**, *131*, 1336.
(7) Paulus, G. L. C.; Wang, Q. H.; Strano, M. S. *Acc. Chem. Res.* **2013**, *46*, 160.
(8) Huang, P.; Jing, L.; Zhu, H.; Gao, X. *Acc. Chem. Res.* **2013**, *46*, 43.
(9) Niyogi, S.; Bekyarova, E.; Itkis, M. E.; Zhang, H.; Shepperd, K.; Hicks, J.; Sprinkle, M.; Berger, C.; Lau, C. N.; deHeer, W. A.; Conrad, E. H.; Haddon, R. C. *Nano Lett.* **2010**, *10*, 4061.
(10) Zhang, H.; Bekyarova, E.; Huang, J.-W.; Zhao, Z.; Bao, W.; Wang, F.; Haddon, R. C.; Lau, C. N. *Nano Lett.* **2011**, *11*, 4047.
(11) Withers, F.; Bointon, T. H.; Dubois, M.; Russo, S.; Craciun, M. F. *Nano Lett.* **2011**, *11*, 3912.
(12) Allongue, P.; Delamar, M.; Desbat, B.; Fagebaume, O.; Hitmi, R.; Pinson, J.; Savéant, J. M. *J. Am. Chem. Soc.* **1997**, *119*, 201.
(13) Anariba, F.; DuVall, S. H.; McCreery, R. L. *Anal. Chem.* **2003**, *75*, 3837.
(14) Brooksby, P. A.; Downard, A. J. *Langmuir* **2004**, *20*, 5038.
(15) Koehler, F. M.; Luechinger, N. A.; Ziegler, D.; Athanassiou, E. K.; Grass, R. N.; Rossi, A.; Hierold, C.; Stemmer, A.; Stark, W. J. *Angew. Chem., Int. Ed.* **2009**, *48*, 224.
(16) Ritzert, N. L.; Rodriguez-Lopez, J.; Tan, C.; Abruna, H. D. *Langmuir* **2013**, *29*, 1683.
(17) Koehler, F. M.; Jacobsen, A.; Ensslin, K.; Stampfer, C.; Stark, W. J. *Small* **2010**, *6*, 1125.
(18) Cougnon, C.; Gohier, F.; Belanger, D.; Mauzeroll, J. *Angew. Chem., Int. Ed.* **2009**, *48*, 4006.
(19) Torbensen, K.; Malmos, K.; Kanoufi, F.; Combellas, C.; Pedersen, S. U.; Daasbjerg, K. *ChemPhysChem* **2012**, *13*, 3303.
(20) Lehr, J.; Garrett, D. J.; Paulik, M. G.; Flavel, B. S.; Brooksby, P. A.; Williamson, B. E.; Downard, A. J. *Anal. Chem.* **2010**, *82*, 7027.
(21) Ebejer, N.; Schnippering, M.; Colburn, A. W.; Edwards, M. A.; Unwin, P. R. *Anal. Chem.* **2010**, *82*, 9141.
(22) Lai, S. C. S.; Dudin, P. V.; Macpherson, J. V.; Unwin, P. R. *J. Am. Chem. Soc.* **2011**, *133*, 10744.
(23) Snowden, M. E.; Güell, A. G.; Lai, S. C. S.; McKelvey, K.; Ebejer, N.; O'Connell, M. A.; Colburn, A. W.; Unwin, P. R. *Anal. Chem.* **2012**, *84*, 2483.
(24) Güell, A. G.; Ebejer, N.; Snowden, M. E.; Macpherson, J. V.; Unwin, P. R. *J. Am. Chem. Soc.* **2012**, *134*, 7258.
(25) Saby, C.; Ortiz, B.; Champagne, G. Y.; Belanger, D. *Langmuir* **1997**, *13*, 6805.
(26) Belanger, D.; Pinson, J. *Chem. Soc. Rev.* **2011**, *40*, 3995.
(27) Patel, A. N.; Tan, S.-Y.; Unwin, P. R. *Chem. Commun.* **2013**, *49*, 8776.
(28) Zoval, J. V.; Stiger, R. M.; Biernacki, P. R.; Penner, R. M. *J. Phys. Chem.* **1996**, *100*, 837.
(29) Miranda-Hernandez, M.; Gonzalez, I.; Batina, N. *J. Phys. Chem. B* **2001**, *105*, 4214.
(30) Lai, S. C. S.; Patel, A. N.; McKelvey, K.; Unwin, P. R. *Angew. Chem., Int. Ed.* **2012**, *51*, 5405.
(31) Anne, A.; Cambril, E.; Chovin, A.; Demaille, C.; Goyer, C. *ACS Nano* **2009**, *3*, 2927.
(32) Downard, A. J. *Langmuir* **2000**, *16*, 9680.
(33) Laforgue, A.; Addou, T.; Belanger, D. *Langmuir* **2005**, *21*, 6855.
(34) Adenier, A.; Combellas, C.; Kanoufi, F.; Pinson, J.; Podvorica, F. I. *Chem. Mater.* **2006**, *18*, 2021.
(35) Pinson, J.; Podvorica, F. I. *Chem. Soc. Rev.* **2005**, *34*, 429.